Supporting Information

N/O-Functionalized MOFs with Nonpolar Channels for Efficient Natural Gas Purification and Carbon Capture

Weiwei Xu [#,a], Xing-Zhe Guo[#,a,c], Nan Ma [a], Zihao Xing[,a], Jiantang Li[*,b], Jinfa Chang[*,a]*
4

[a] Key Laboratory of Polyoxometalate and Reticular Material Chemistry of Ministry of Education, Faculty of Chemistry, Northeast Normal University, Changchun 130024, P. R. China. E-mail: xingzh612@nenu.edu.cn; changjinfa@nenu.edu.cn.

[b] Key Laboratory of the Ministry of Education for Advanced Catalysis Materials, College of Chemistry and Materials Sciences, Zhejiang Normal University, Jinhua, 321004, PR China. E-mail: jiantang.li@zjnu.edu.cn

[c] State Key Laboratory of Solid Lubrication, Lanzhou Institute of Chemical Physics, Chinese Academy of Sciences
Lanzhou, 730000 China

[#]W. Xu and X-Z. Guo contributed equally to this work

Experimental

All reagents were used as received without purification. Thermogravimetric analysis (TGA) was carried out on a simultaneous DSC-TGA SDT 650 thermal analyzer heated from 25°C to 800°C under a nitrogen atmosphere with a heating rate of 10 °C min^{-1}. Powder X-ray diffraction patterns (PXRD) were recorded on a Rigaku Smartlab SE powder diffractometer using Cu-Kα (λ = 1.54056 Å). Single component adsorption measurements of N_2, CO_2, CH_4, C_2H_6 and C_3H_8 were performed on a Quantachrome AutoSorb iQ analyzer. Breakthrough curves were obtained using a BSD-MAB multi-constituent adsorption breakthrough curve analyzer.

Synthesis of PyC-Zn-MOF

A mixture of $Zn(NO_3)_2 \cdot 6H_2O$ (50.0 mg),1H-Pyrazole-4-carboxylic acid (12.0 mg), and Purin-6-amine (10.0 mg) was dissolved in N,N-Dimethylformamide (DMF)/H_2O (9 mL, 8:1 v/v). This solution was transferred to a 15 mL pressure-resistant flask containing 2-Imidazolidone (1.50 g). The reaction vessel was then sealed and heated at 120°C for 3 days. Upon cooling to room temperature, the resulting crystalline solid was collected and washed with ethanol, yielding colorless crystals.

Single-component gas sorption experiments

All sorption isotherms for N_2, CH_4, C_2H_6, C_3H_8 and CO_2 at 298 / 273 K, and N_2 at 77 K were collected using a Beishide Instrument BSD-660 analyzer. All high-purity gases used in the single-gas adsorption experiments were purchased commercially: He (99.999%), C_2H_6 (99.99%), C_3H_8 (99.9%), CH_4 (99.999%), CO_2 (99.99%), N_2 (99.999%). Before the single-gas sorption experiments, the sample was activated under high vacuum at 120°C for 12 hours. When measuring the N_2 adsorption isotherm, the temperature was maintained at 77 K using a Dewar flask containing liquid N_2. The sample was regenerated by degassing at 120°C under high vacuum for 6 hours between the measurement of each independent isotherm.

Breakthrough experiments

All breakthrough tests were performed on the JWGB MIX 100 equipment and conducted using a quartz column (3 mm inner diameter 8 cm) manually packed with PyC-Zn-MOF. The samples (wight: 413.5 mg) in the column were first activated with Helium flow (10 mL min-1) for 12 h at 353 K. The mixed gases (binary equimolar CO_2/N_2 (50/50, v/v) and ternary gas mixture $CH_4/C_2H_6/C_3H_8$ (85%/10%/5%, v/v) were then introduced at 2 mL min^{-1} at 298 K. After each breakthrough experiment, the sample was regenerated with Helium flow of 10 mL min^{-1} under 333 K for 3 h.

GCMC Simulation

To calculate adsorption performance in PyC-Zn-MOF, grand canonical Monte Carlo (GCMC) simulations were performed using the RASPA package (D. Dubbeldam, S. Calero, D.E. Ellis, R.Q. Snurr, *Mol. Simulat.* 2016). During the simulation, the MOF is treated as rigid framework and the GenericMOFs force field is used [11]. For the gas molecules, potential parameters are taken from the TraPPE force field. A cutoff distance of 12 Å was set for the Lennard-Jones (LJ) interactions, and all unit cells were sufficiently replicated to avoid interactions between periodic replicas. Long-range electrostatic interactions were treated with the Ewald summation method. For each state point, GCMC simulations consisted of 100,000 steps for equilibration, followed by 100,000 steps for sampling the desired thermodynamic properties.

Isosteric heat of adsorption

A virial-type expression comprising temperature-independent parameters a_i and b_j was employed to calculate the enthalpies of adsorption for C_2H_6, C_3H_8, CH_4, and CO_2 on PyC-Zn-MOF. In each case, the data were fitted with equation:

$$\ln P = \ln N + 1/T \sum_{i=0}^{m} a_i N^i + \sum_{i=0}^{n} b_i N^i \quad \textbf{(1)}$$

Here, P is the pressure expressed in Pa, N is the amount absorbed in mmol g^{-1}, T is the temperature in K, a_i and b_j are virial coefficients, and m, n represent the number of coefficients required to adequately describe the isotherms (m and n were gradually increased until the contribution of extra added a and b coefficients was deemed statistically insignificant to the overall fit, minimizing the average squared deviation from the experimental values). The values of the virial coefficients a_0 to a_m were then used to calculate the isosteric heat of adsorption utilizing the following expression:

$$Q_{st} = -R \sum_{i=0}^{m} a_i N^i \quad \textbf{(2)}$$

Q_{st} is the coverage-dependent isosteric heat of adsorption and R is the universal gas constant. The heats of adsorption for C_2H_6, C_3H_8, CH_4 and CO_2 on PyC-Zn-MOF were determined using sorption data measured in the pressure range from 0 to 1 bar at 273 K and 298 K.

Selectivity prediction for binary mixture adsorption

The ideal adsorbed solution theory (IAST) was used to predict binary mixture adsorption from the experimental pure-gas isotherms. The experimental isotherm data for

pure N_2, C_2H_6, C_3H_8, CO_2 and CH_4 were fitted using a single-site Langmuir-Freundlich equation model:

$$\mathbf{q} = \mathrm{a}\frac{b * p^c}{1 + b * p^c} \qquad \textbf{(3)}$$

where q and p are the adsorbed amounts and the equilibrium pressure of component i, respectively.

The adsorption selectivities for binary mixtures of CO_2/N_2, C_2H_6/CO_2 and C_3H_8/CH_4, defined by

$$S_{\mathrm{i/j}} = \frac{x_{\mathrm{i}} * y_{\mathrm{j}}}{x_{\mathrm{j}} * y_{\mathrm{i}}} \qquad \textbf{(4)}$$

where x_i is the mole fraction of component i in the adsorbed phase and y_i is the mole fraction of component i in the bulk gas phase, were calculated using IAST.

Supplementary Figures

Figure S1. Crystalline particles of PyC-Zn-MOF.

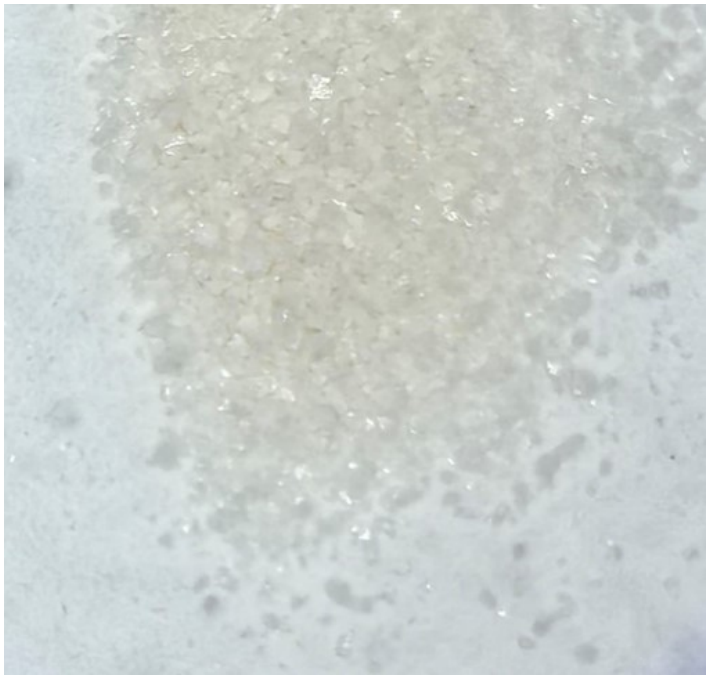

Figure S2. Optical micrograph of PyC-Zn-MOF.

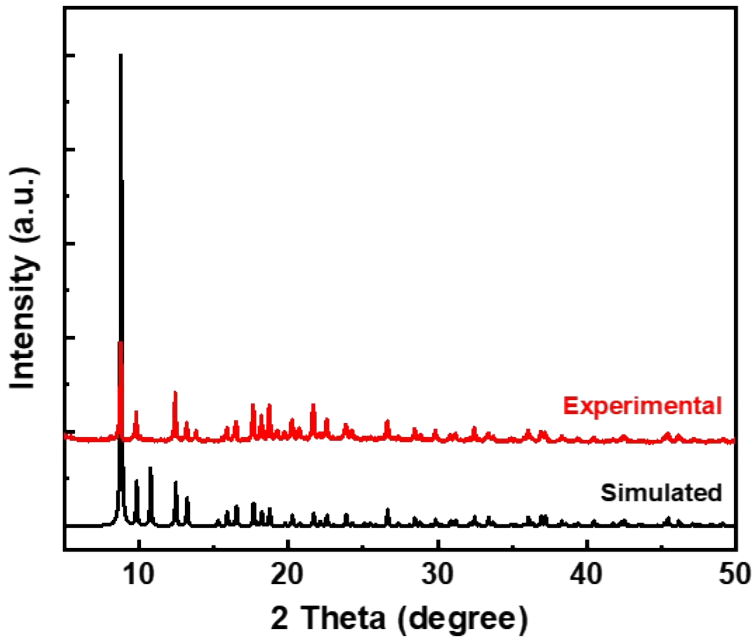

Figure S3. PXRD pattern of PyC-Zn-MOF.

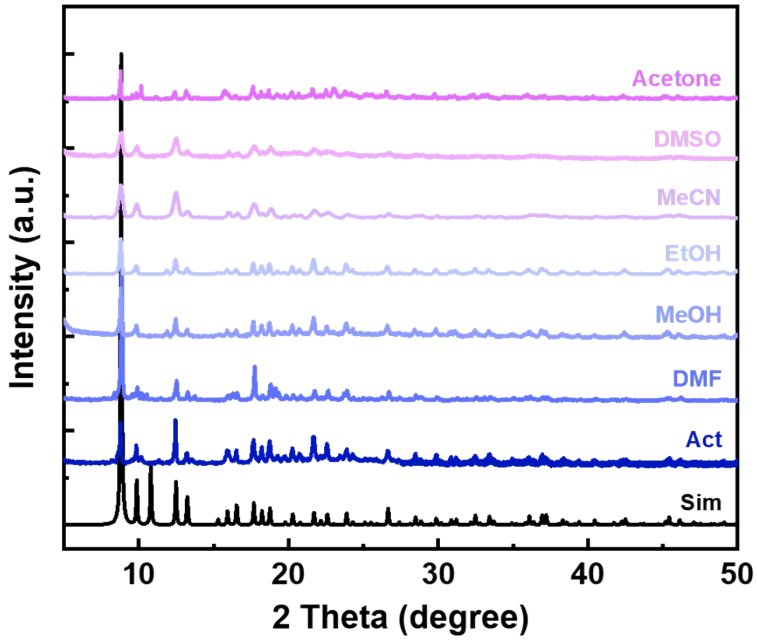

Figure S4. Powder X-ray powder diffraction patterns of PyC-Zn-MOF.

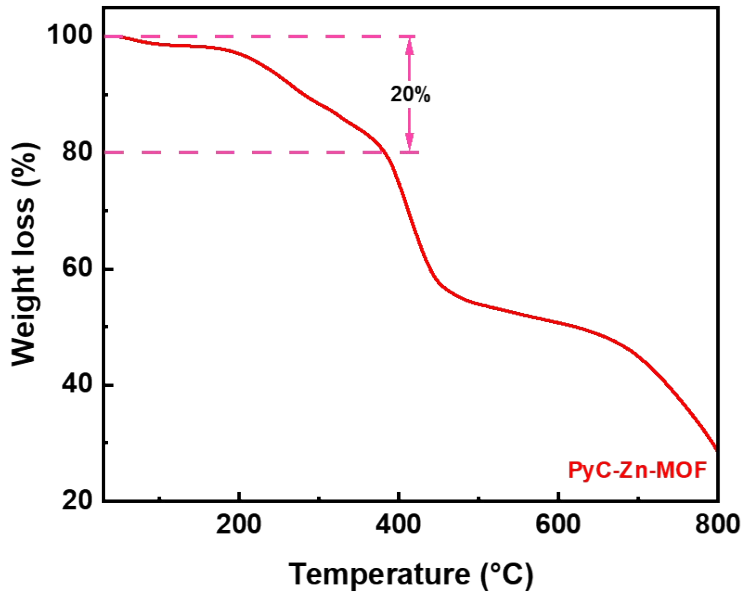

Figure S5. TGA curve of PyC-Zn-MOF.

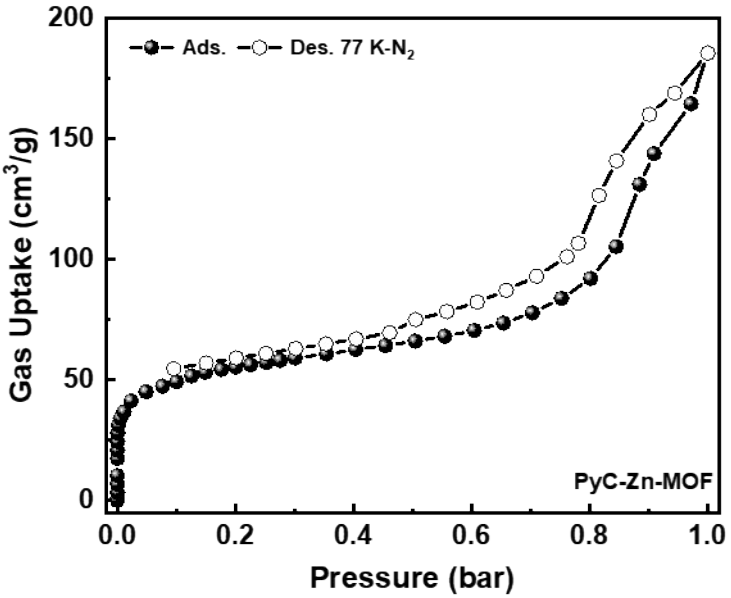

Figure S6. N_2 adsorption-desorption isotherm of PyC-Zn-MOF at 77 K.

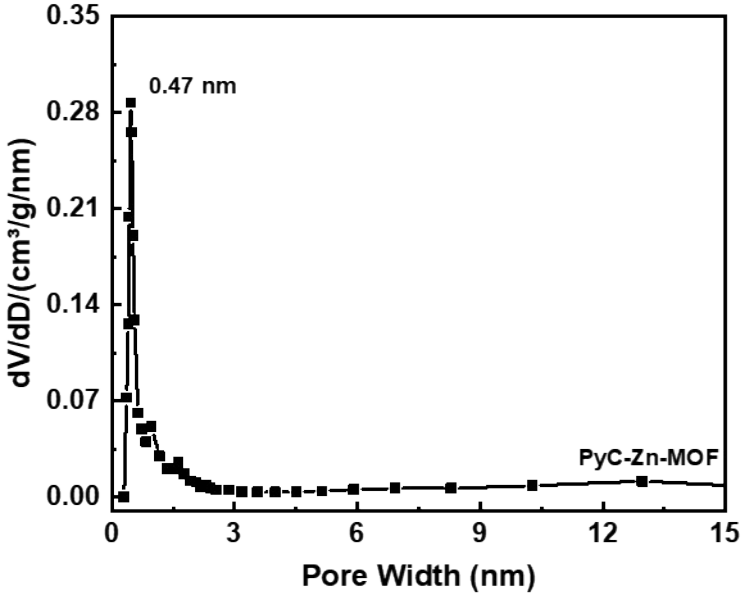

Figure S7. Corresponding pore size distribution of PyC-Zn-MOF at 77 K.

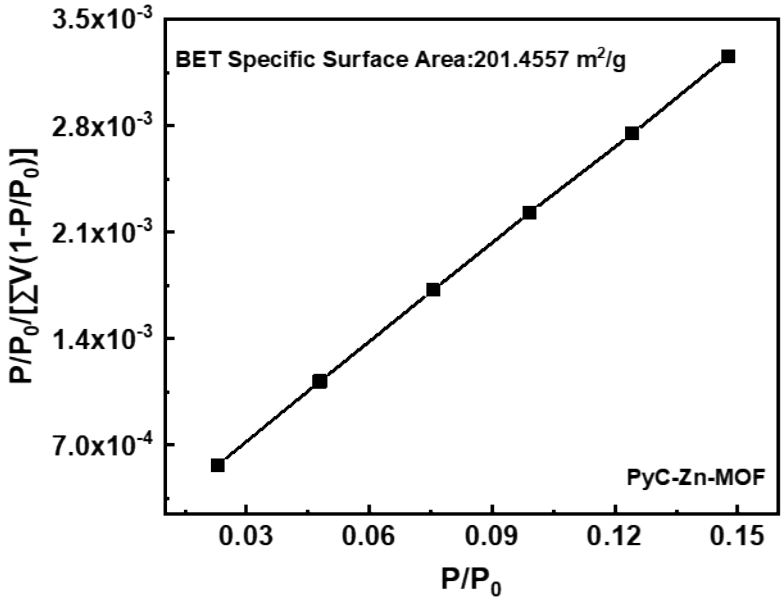

Figure S8. BET surface area plot derived from N_2 adsorption isotherm at 77 K.

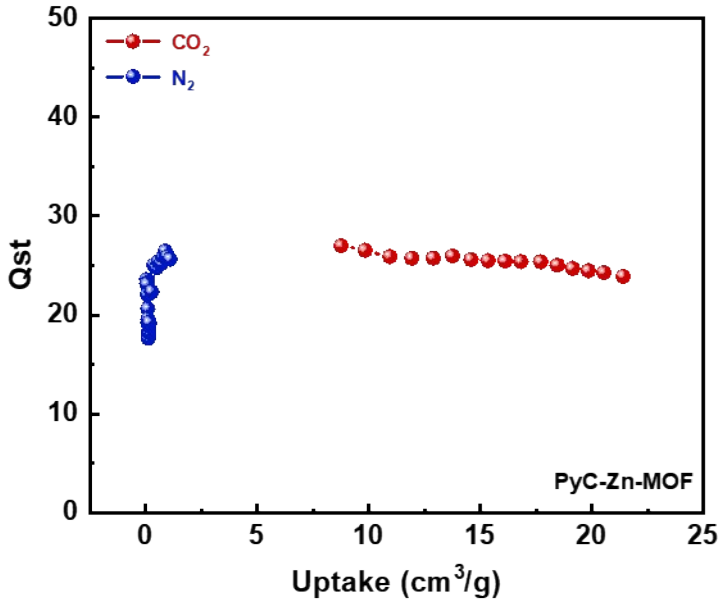

Figure S9. Isosteric heats of adsorption for CO_2 and N_2 on PyC-Zn-MOF.

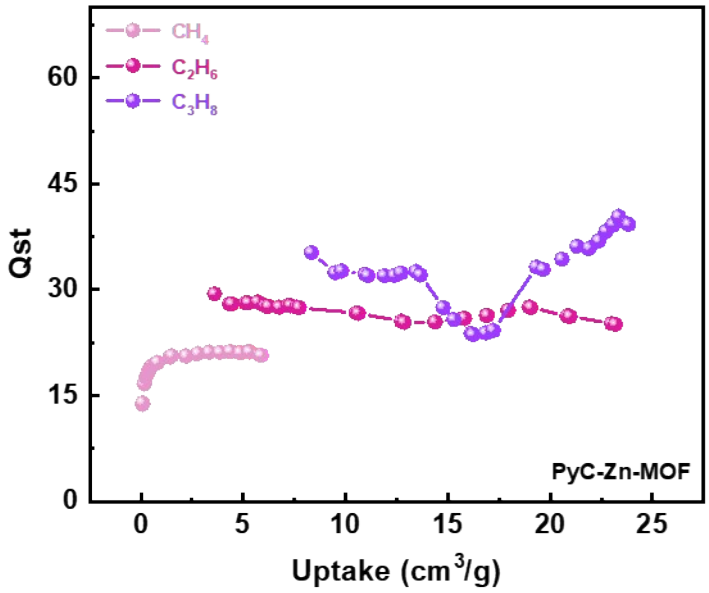

Figure S10. Isosteric heats of adsorption for CH_4, C_2H_6 and C_3H_8 on PyC-Zn-MOF.

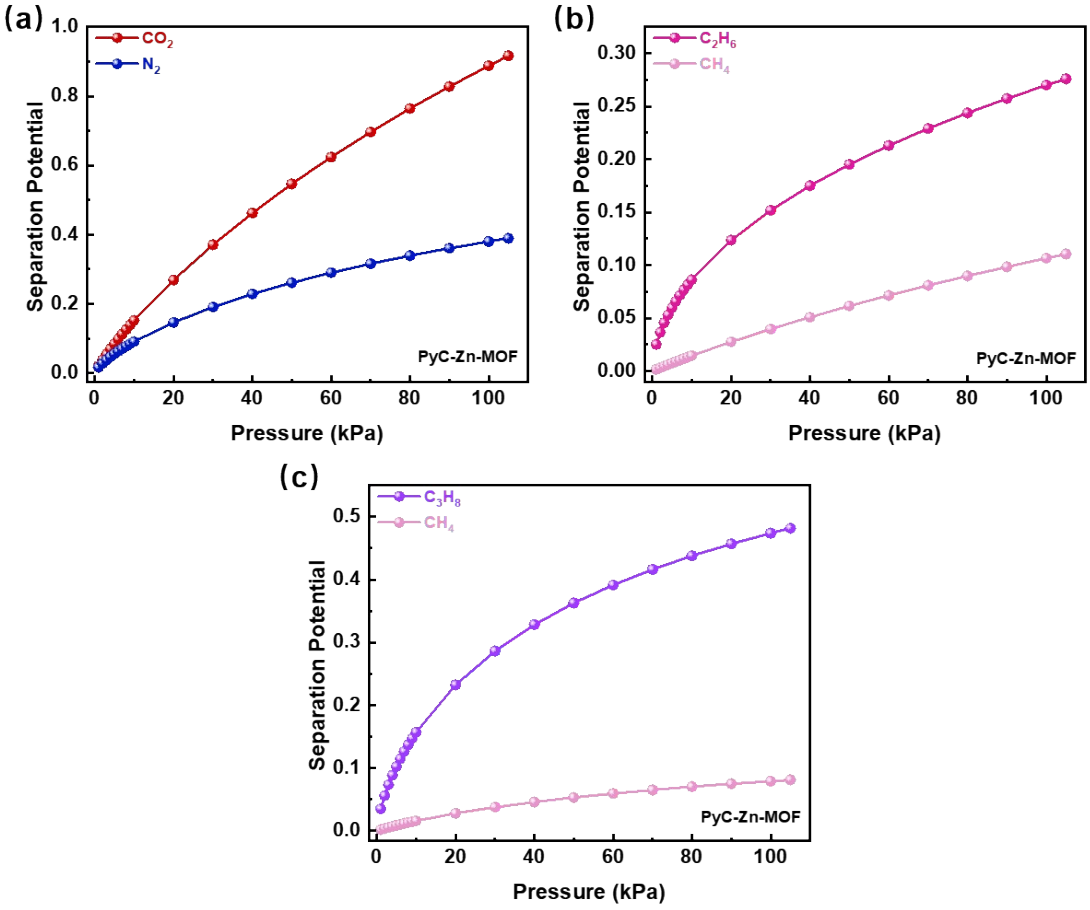

Figure S11. Comparison of q-values for different gas mixtures: (a) CO_2/N_2 (50/50), (b) C_2H_6/CH_4 (10/85), and (c) C_3H_8/CH_4 (5/85).

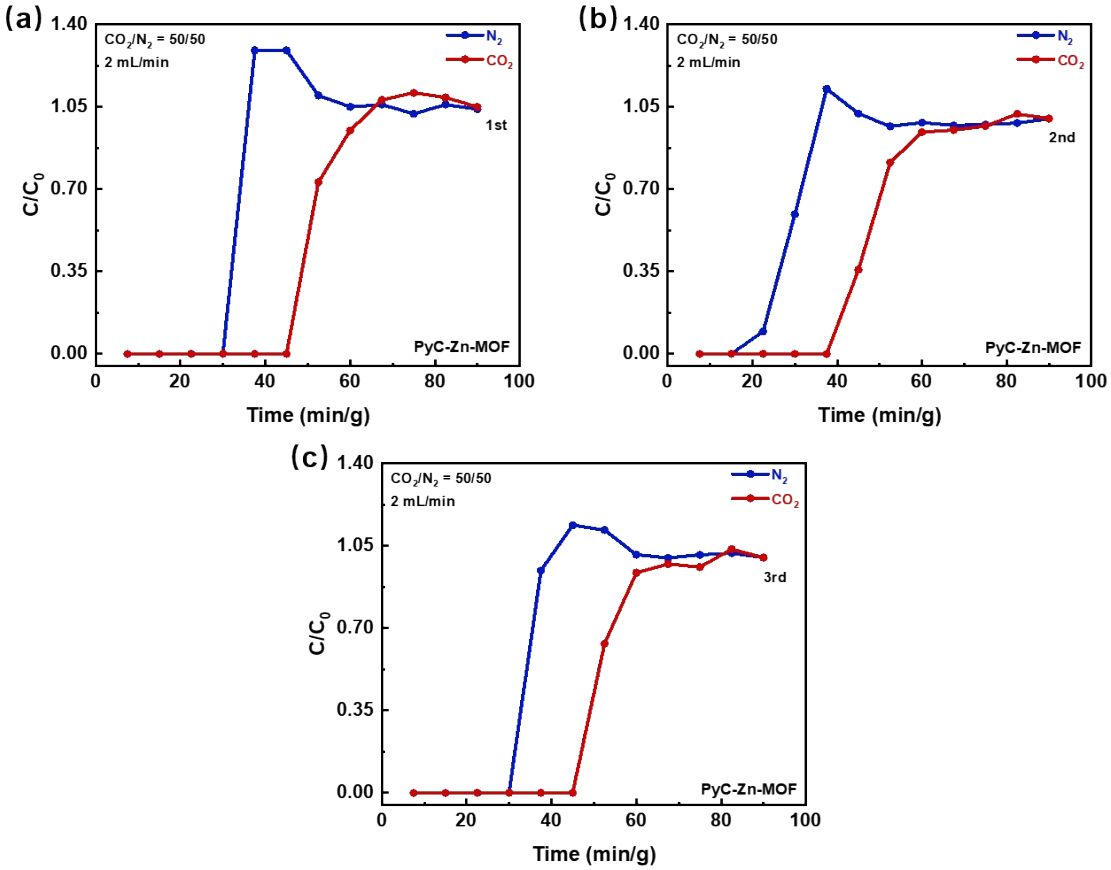

Figure S12. Recyclability test of dynamic breakthrough curves for three consecutive cycles of a CO_2/N_2 (50/50, v/v) mixture on PyC-Zn-MOF: (a) first cycle, (b) second cycle, (c) third cycle.

Supplementary Tables

Table S1. Calculated electrostatic potential values for gas molecules and the PyC-Zn-MOF framework.

Structure	Charge
C_2H_6	$-5.189e^{-3}$
C_3H_8	$-6.882e^{-3}$
CH_4	$-8.023e^{-3}$
CO_2	$-3.57e^{-2}$
N_2	$-1.734e^{-2}$

Table S2. Comparison of CO_2 adsorption capacities for various porous materials at 298 K and 10 kPa.

Material	CO_2 adsorption (cm^3/g)	References
MOF@CP-0	5.69	Advanced Sustainable Systems, 2024, 8, 2300466
CoIPA	4.95	AIChE Journal, 2017, 63, 4532-4540
PyC-Zn-MOF	4.56	This work
SU-102	4.47	Chemical Engineering Journal, 2024, 502, 157956
PCN-222	4.09	Industrial & Engineering Chemistry Research, 2018, 57, 12215-12224
$[Zn^{II}(L)BPY]$	3.64	Dalton Transactions, 2021, 50, 2880-2890
MIP-202	3.14	Chemical Engineering Journal, 2019, 375, 122074
Ca-MOF-1	2.85	Dalton Transactions, 2024, 53, 11120-11132
MAF-7	2.72	Advanced materials, 2011, 23, 1268-1271

Mg-MOF-74	2.59	Colloids and Surfaces A: Physicochemical and Engineering Aspects, 2025, 710, 136223
$[Mn(NCPP)]_n$	1.81	Chemical Communications, 2020, 56, 13377-13380

Table S3. Comparison of C_2H_6/CH_4 and C_3H_8/CH_4 adsorption selectivity for various porous materials at 298 K and 100 kPa.

Material	**C_2H_6/CH_4**	**C_3H_8/CH_4**	**References**
PyC-Zn-MOF	21.5	102	This work
TPOA-F	17.7	99	New Journal of Chemistry, 2023, 47, 17567-17577
UTSA-35a	20	80	Chemical Communications, 2012, 48, 6493-6495
InOF-1	17	90	Industrial & Engineering Chemistry Research, 2017, 56, 4488-4495
DMOF-F	9.5	80.4	Dalton Transactions, 2023, 52, 15462-15466
JUC-106	13	75	Chemistry–A European Journal, 2014, 20, 9073-9080
Zn-BPZ-SA	10.5	40.6	ACS Materials Letters, 2023, 5, 1091-1099
MFM-202a	10	87	Chemistry of Materials, 2016, 28, 2331-2340
JLU-Liu21	7	99.2	Chemical Communications, 2016, 52, 3223-3226
ZUL-C1	22	73	Journal of the American Chemical Society, 2022, 144, 14322-14329
sPI-M-H	13.9	82	ACS applied materials & interfaces, 2018, 10, 26618-26627
HPC800-1.5	15	91	Chemical Engineering Journal, 2022, 428, 130985

UC800	9.1	41.8	ACS Sustainable Chemistry & Engineering, 2020, 8, 11721-11728
A-AC-3	16.9	77	Separation and Purification Technology, 2018, 190, 60-67
NUM-18a	19.7	109	Separation and Purification Technology, 2023, 304, 122312